Discover Oncology

Research

Prognostic alternative splicing and multi-omics characteristics reveal *FTCD* is a potential target of hepatocellular carcinoma

Yanli Zhang[1,2] · Wenxing Li[3,4] · Mengyi Sun[5] · Lisheng Zhang[1]

Received: 23 February 2024 / Accepted: 26 July 2024
Published online: 27 November 2024

Abstract

Objective This research aimed to identify alternative splicing (AS) variants in hepatocellular carcinoma (HCC) and assess their prognostic biomarker potential. We analyzed genome-wide prognostic-associated AS events to pinpoint specific genes that could predict HCC patient outcomes and serve as therapeutic targets.

Methods Analyzing 343 liver cancer samples from The Cancer Genome Atlas (TCGA) via RNA-seq, we evaluated the impact of seven AS patterns on HCC. We constructed a prognostic prediction model using Cox proportional hazards regression and developed a splicing network by correlating survival-associated AS events with splicing factor expression. Notably, we investigated Formiminotransferase cyclodeaminase (*FTCD*) gene for its role in liver cancer cell proliferation and pathway mechanisms in mice and cell models.

Results We discovered 3164 survival-associated AS events, with the top 20 mostly indicating poor prognosis. Our prognostic model, integrating various AS patterns, demonstrated robust performance in stratifying HCC risk (AUC = 0.830). Splicing network analysis highlighted significant correlations between splicing factors and AS events. Lower expression of *FTCD*, associated with adverse HCC outcomes, was found to regulate cell proliferation via the *PI3K/AKT/mTOR* pathway.

Conclusion This study offers a prognostic prediction model for HCC patient risk stratification, identifying the *FTCD* gene as a crucial prognostic marker and therapeutic target. This highlights *FTCD*'s potential impact on HCC clinical diagnosis and treatment strategies.

Keywords Alternative · Splicing · Hepatocellular carcinoma · Prognosis · *FTCD* · *mTORC1*

1 Introduction

Hepatocellular carcinoma (HCC) is a predominant form of liver cancer, accounting for approximately 90% of all cases. It is recognized as the third most common cause of cancer-related mortality on a global scale [1–3]. The considerable prevalence of HCC emphasizes its substantial impact on global health, emphasizing the immediate requirement for effective prevention, early detection, and treatment approaches to address this disease. The liver, an essential organ responsible for digestion, metabolism, and detoxification processes within the body, plays a pivotal role in energy

Supplementary Information The online version contains supplementary material available at https://doi.org/10.1007/s12672-024-01201-y.

✉ Yanli Zhang, yanli2109@126.com | [1]College of Veterinary Medicine/College of Biomedicine and Health, Huazhong Agricultural University, Wuhan 430070, Hubei, China. [2]Technology Center for Protein Sciences, Tsinghua University, Beijing 100084, China. [3]Department of Clinical Medicine, Heze Medical College, Heze 274000, Shandong, China. [4]Department of Surgery, Affiliated Hospital of Heze Medical College, Heze 274000, Shandong, China. [5]Beijing Pharma and Biotech Center, Beijing 100035, China.

metabolism and the elimination of toxins. Nonetheless, the infiltration of malignant tumor cells disrupts the liver's regular metabolic functions, resulting in a range of symptoms, including jaundice, pain, and weight loss. These symptoms can be life-threatening and significantly impact the overall well-being of patients [4]. Despite notable advancements in cancer research, there remains a lack of comprehensive understanding regarding the molecular mechanisms that underlie the initiation and progression of HCC. This knowledge gap is primarily attributed to the heterogeneity of the tumor and the presence of various risk factors associated with HCC [5]. Therefore, further research is needed to unravel the intricate molecular pathways involved in HCC, which can pave the way for the development of targeted therapies and improved clinical management strategies for this aggressive form of cancer.

Alternative splicing (AS) is a critical mechanism that governs gene expression by modulating the translation of distinct mRNA variants, thereby contributing to the generation of protein diversity. This process is essential for the abundance and diversity of protein isoforms [6–10]. AS encompasses seven distinct splicing patterns, including exon skip (ES), alternate terminator (AT), Alternate promoter (AP), alternate acceptor (AA), alternate donor (AD), retained intron (RI), and mutually exclusive exons (ME). In normal physiological processes, genes undergo alternative splicing, producing different splice variants [11]. However, compared to normal cells, cancer cells often exhibit a higher frequency of splicing changes. Aberrant AS events are closely associated with cancer progression, metastasis, treatment resistance, and other carcinogenic processes. Mutations or alterations in the expression of splicing factors can lead to the activation of oncogenes and cancer pathways, or the loss of tumor suppressor functions [12–15]. Numerous studies have highlighted the importance of AS in the progression of liver cancer. Zhou et al. performed RNA sequencing on nine pairs of primary HCC tissues with extrahepatic metastasis and nine pairs of metastasis-free HCC tissues, depicting the landscape of AS in HCC and found a higher frequency of AS events in HCC tissues with extrahepatic metastasis compared to those without metastasis [16]. A recent study identified *LINC01089* as a super enhancer-driven lncRNA that induces *ERK* signaling and epithelial-mesenchymal transition by regulating *DIAPH3* alternative splicing that blocks N6-methyladenosine-mediated mRNA stabilization, promoting epithelial-mesenchymal transition, migration, invasion, and metastasis of HCC cells in vivo and in vitro [17]. Increasing evidence suggests that dysregulation of splicing events and cancer-specific splice variants can serve as prognostic biomarkers and therapeutic targets for HCC [5, 18–21]. Therefore, establishing the correlation between aberrant splicing and HCC is a pivotal inquiry in the field of cancer research. However, comprehensive studies on AS events associated with HCC survival are still lacking. Therefore, there is an urgent need to employ transcriptomic approaches to explore survival-related AS events in HCC patients and evaluate their potential prognostic value. This research can provide valuable insights into the molecular mechanisms underlying HCC progression and identify novel targets for prognosis prediction and therapeutic interventions.

In this study, our initial approach involved analyzing RNA-seq data from a cohort of 343 patients with HCC in the TCGA database, aiming to investigate the role of differential AS patterns and gain systematic insights into the prognostic impact of AS events on patient survival. By conducting a prognostic prediction model and developing a splicing network by correlating survival-associated AS events with splicing factor expression, we can elucidate the variations in RNA splicing patterns and their potential implications as prognostic biomarkers in HCC. Additionally, a investigation into the role of Formiminotransferase cyclodeaminase (*FTCD*) gene in HCC was conducted, encompassing bioinformatics analyses as well as in vivo and in vitro experiments. *FTCD*, a recently discovered human gene located on chromosome 21q22.3, encodes the enzyme formiminotransferase cyclodeaminase, which plays a crucial role in connecting histidine breakdown to folate metabolism in intermediate metabolism. Multiple cDNAs have been identified, potentially generating three distinct protein isoforms through alternative splicing [22]. *FTCD* shows significant expression levels in both fetal and adult human liver tissues. The purpose was to elucidate the specific involvement of *FTCD* in HCC and its potential significance as a prognostic biomarker and to develop novel and targeted therapeutic approaches for HCC. Our study aimed to elucidate the complexities of RNA splicing patterns and decipher the functional consequences of splice variants, with the ultimate goal of offering valuable insights that can guide the development of novel treatment strategies for HCC.

2 Materials and methods

2.1 Data acquisition and treatment

To acquire the necessary data for our study, we accessed RNA-seq data and clinical information from a cohort of 343 patients with HCC. The data was obtained from TCGA portal, which can be accessed at https://portal.gdc.cancer.gov/.

2.2 Construction of mice model

The animal experiments were conducted in accordance with the ethical guidelines set by the Huazhong Agricultural University Ethics Committee (No. [2023] 020423). The mice were kept in a controlled environment with a temperature of 20–22 °C, a 12-h light/dark cycle, humidity maintained at 50–70%, and access to food and water ad libitum. We procured 5–6-week-old nude mice and established subcutaneous tumor-bearing nude mice models (n = 5 in each group). The process involved digesting the drug-treated BEL-7402 liver cancer cell line using 0.25% trypsin and obtaining a cell pellet through centrifugation. Subsequently, the cells were resuspended in physiological saline, and cell counting was performed to achieve a cell concentration of 10^6 cells/0.1 mL. After disinfecting the inguinal region with an alcohol swab, 0.1 mL of the cell suspension was aspirated and injected subcutaneously into the nude mice. To ensure proper subcutaneous injection rather than intradermal or intramuscular injection, the needle tip was slightly moved left and right, confirming the absence of resistance. The subcutaneous tumor-bearing nude mice were then randomly divided into three groups: the saline group (CK group), the BEL-7402 liver cancer cell line group (H group), and the BEL-7402 liver cancer cell line overexpressing FTCD group (F group). The drugs were administered every 2 days via intratumoral injection. Fifteen days later, the nude mice were anesthetized using 1% pentobarbital and euthanized. The liver tissues from each group of nude mice were dissected and collected for further analysis.

In our study, we adhered to the maximum tumour size/burden set by the Animal Ethics Committee of Huazhong Agricultural University of China of not exceeding 2000 mm^3, which corresponds to a diameter of not more than 20 mm. All animal subjects were closely monitored, and tumour measurements were recorded regularly to ensure compliance. In this study, we confirmed that the tumour size/burden did not exceed the limits set by the ethics committee at all times. In the event of any deviations, corrective measures were taken immediately to safeguard the welfare of the animals and the justification for these was documented in detail in the study report.

2.3 Cell model construction

The normal liver cell line HL-7702 and the liver cancer cell line BEL-7402 were obtained from ATCC. These cell lines were cultured in RPMI-1640 medium (PM150110) supplemented with 10% fetal bovine serum (FBS) (164210-500) at 37 °C with 5% CO_2.To establish the FTCD overexpressing cell line, the *FTCD* overexpression plasmid was transfected into logarithmic phase BEL-7402 cells. After washing the cells with phosphate-buffered saline (PBS) and digesting them with trypsin, the cells were seeded in a 6-well plate and incubated for 24 h. The cell fusion rate was observed under a microscope, and transfection was performed when the fusion rate reached 40%. In the 6-well plate, the original culture medium was removed, and the wells were washed 1–2 times with PBS buffer. Then, 500 µL of serum-free basic culture medium was added to each well. Eight µL Lipofectamine™ 3000 (Invitrogen) transfection reagent, 4 µg *FTCD* overexpression plasmid DNA, and 500 µL serum-free medium were mixed to prepare the transfection reagent. The transfection reagent was added sequentially to each well of the 6-well plate for transfection. The normal liver cell line HL-7702 was used as the Control group, the liver cancer cell line BEL-7402 was used as the HCC group, and the BEL-7402 cells transfected with the *FTCD* overexpression plasmid were used as the FTCD group.

2.4 Immunohistochemical analysis of FTCD protein expression in mice liver tissue

In the analysis of FTCD protein expression in mice liver tissue, the FTCD Polyclonal Antibody (ThermoFisher, PA5-115255) was procured. Mice liver tissue samples were fixed in 10% neutral buffered formalin and subsequently embedded in paraffin to generate sections measuring 4–6 µm in thickness. Antigen retrieval was performed by utilizing citrate buffer, followed by a blocking treatment. The samples were then subjected to incubation with the FTCD Polyclonal Antibody at a dilution of 1:100 for a duration of 1.5 h at a temperature of 22 ℃. Subsequently, a secondary staining was carried out using HRP-labeled rabbit anti-secondary antibody, and the samples were visualized under an optical microscope.

2.5 CCK-8 (cell counting kit-8)

The proliferation ability of cells was assessed using the CCK-8 assay kit (Yeasen, 40203ES60, China). The presence of a higher number of viable cells in the culture wells corresponds to an increased abundance of dehydrogenases. These dehydrogenases act upon the WST-8 reagent in the CCK-8 assay kit, leading to the formation of a yellow formazan product. The intensity of the resulting color is directly proportional to the cell viability, with a darker color indicating higher viability. For the experimental procedure, cells in the Control group, HCC group, and FTCD group were enzymatically detached using trypsin, and a cell suspension was obtained and quantified. After performing cell counting, the cells were appropriately diluted using fresh cell culture medium to achieve a concentration of 5000 cells per 100 µL. Subsequently, the diluted cells were carefully seeded into a 96-well plate and placed in a dedicated cell incubator (37 °C, 5% CO_2) for 24 h. Following the specified incubation time (24 h, 48 h, 72 h and 96 h), 10 µL CCK-8 was added to the cell. Four hours later, the cell viability was evaluated by measuring the absorbance at a wavelength of 450 nm.

2.6 Quantitative real-time PCR

Total RNA was extracted from the samples, and cDNA synthesis was performed using a commercially available reagent kit (Invitrogen, United States). *GAPDH* served as the housekeeping gene for normalization. The forward primer sequence for *FTCD* was GGAATGCGTCCCCAACTTTTC, and the reverse primer sequence was TGTCGATAAGTCGGGAAGCTAC. The forward primer sequence for *PPAR* was AACTGCAGGGTGAAACTCTGGGAGATTCTCC, and the reverse primer sequence was GGATTCAGCAACCATTGGGTCAGCTCT. The forward primer sequence for *PI3KCA* was CTATTCGACAGCATGCCAATC TCTTCAT, and the reverse primer sequence was TTAACAGTGCAGTGTGGAATCCAGAGTG. The forward primer sequence for *AKT* was ATGAGCGACGTGGCTATTGT, and the reverse primer sequence was GAGGCCGTCAGCCACAGTCT. The forward primer sequence for *PTEN* was GACGGGAAGACAAGTTCAT and the reverse primer sequence was GGTTTCCTCTGGTCC TGGT. As for *GAPDH*, the forward primer sequence was CTGGGCTACACTGAGCACC, and the reverse primer sequence was AAGTGGTCGTTGAGGGCAATG. In the PCR amplification process, 1.0 µL of cDNA was utilized as the template. The PCR program encompassed 40 cycles, with denaturation carried out at 95 °C for 30 s, annealing at 58 °C for 30 s, and extension at 72 °C for 30 s in each cycle. The relative expression level of the *FTCD* gene was analyzed using the ΔΔCt method, which enables comparison between various experimental conditions. This method involves calculating the difference in Ct values between the target gene (*FTCD*) and a reference gene (*GAPDH*), and then comparing this difference between different experimental groups to determine the relative expression level.

2.7 Western blot

The cells were digested using a 0.25% trypsin solution, and the resulting cell pellet was obtained through centrifugation. To prepare the cell lysis buffer, PMSF and RIPA lysis buffer were mixed in a 1:100 ratio. An appropriate volume of the cell lysis buffer was added to the cell pellet and incubated on ice for 30 min. Following centrifugation, the supernatant was carefully transferred to a new EP tube and stored for subsequent analysis. The protein concentration in the extracted samples was determined, and the proteins were denatured at high temperature. Subsequently, the denatured protein samples underwent electrophoresis, followed by transfer onto a PVDF membrane. Upon completion of the transfer, the PVDF membrane was incubated with a prepared blocking solution containing BSA at room temperature for 1 h. The blocking solution was then collected, and the PVDF membrane was further incubated overnight at 4 °C with a primary antibody appropriately diluted to the desired concentration. After collecting the primary antibody, the PVDF membrane was washed 2–3 times with PBST buffer, each wash lasting for 10 min. Subsequently, the PVDF membrane was incubated with a secondary antibody diluted to the appropriate concentration for 2 h. The secondary antibody was collected, and the PVDF membrane was washed 3 times with PBST solution for 10 min per wash. Finally, the GeneSnap imaging system from SynGene was employed to capture images of the stained proteins.

2.8 Statistical and survival analysis

For the analysis of AS profiles, we utilized the SpliceSeq tool. AS events were quantified using PSI (percent spliced in), a measure commonly employed to quantify the extent of AS.

We conducted an evaluation to assess the clinical significance of various AS events on the overall survival (OS) of patients diagnosed with HCC using univariate Cox regression models. In this analysis, each AS event was treated as an independent variable, while OS served as the dependent variable. The objective was to determine the individual impact of each AS event on patient survival. Furthermore, we performed multivariate Cox regression analysis to identify independent prognostic factors among the seven AS events. These independent prognostic factors, which exhibited significant associations with patient survival, were then utilized as independent variables, while OS remained the dependent variable. This comprehensive analysis aimed to identify the AS events that independently contribute to the prognostic outcome, while considering potential confounding factors.

To compare the prognostic factors for OS within a 5-year period in HCC patients, we employed Kaplan–Meier curves. The patients were divided into high-risk and low-risk groups based on the prognostic factors, and survival curves were plotted. Additionally, a chi-square test was performed to examine the differences in survival status between the high-risk and low-risk groups, thereby validating the effectiveness of the prognostic factors. The R software package was used to conduct receiver operating characteristic (ROC) analysis, enabling a comparison of the predictive performance of each survival model. The accuracy and reliability of the survival models were evaluated by calculating the area under the ROC curve (AUC).

To quantitatively analyze the intersections among the seven survival-associated AS events in HCC, UpSet plots were utilized. Co-expression genes were identified using the KEGG database. Protein–protein interaction information was obtained from the STRING Database, and gene network analysis was performed using Cytoscape to select hub genes among the AS event genes associated with survival. A splicing-related network was constructed in HCC to illustrate the relationship between the expression of splicing factor genes and the PSI values of survival-associated AS events. The correlation was visualized using Cytoscape. All statistical analyses were conducted using R, and a p-value < 0.05 was considered statistically significant.

The functional validation data for the *FTCD* gene were subjected to statistical analysis using SPSS 20.0 software and graphical representation using GraphPad Prism 7.0 software. A significance level of $p < 0.05$ was used to determine statistical significance.

3 Results

3.1 The Cox analysis to investigate the prognostic significance of AS events in HCC cohort

In a comprehensive study involving 343 patients with HCC, a total of 26,157 AS events originating from 12,817 genes were identified. On average, each gene exhibited two AS events. Among the various types of AS events, ES was the most prevalent, followed by AT and AP events. Specifically, 9409 ES events were detected across 4070 genes, 6009 AT events were observed in 2636 genes, and 4874 AP events were identified in 1971 genes. Additionally, 2141 AA events were found in 1538 genes, 1865 AD events were present in 1308 genes, 1795 RI events were detected in 1231 genes, and 64 ME events were observed in 63 genes (Fig. 1).

To evaluate the prognostic significance of AS events in HCC patients, Cox univariate survival analysis was performed. This analysis aimed to assess the impact of each AS event on OS. The results indicated that out of the 26,157 AS events identified, 3164 of them were found to be significantly associated with OS in HCC patients ($p < 0.05$). These significant AS events may potentially serve as prognostic markers for HCC patients. For more detailed information on the specific AS events and their associations with OS, please refer to Table s01.

Figure 2 depicts the 20 most notable AS events associated with survival across the seven types of AS events. A clear observation from the figure is that the majority of these AS events are linked to unfavorable prognostic outcomes. Notably, it is evident that a single gene in HCC can exhibit multiple AS events that are associated with survival. To visually represent the overlap between the seven types of AS events in HCC, researchers generated an UpSet plot (Fig. 3A). Remarkably, a significant proportion of genes associated with survival exhibited at least two types of AS events, with some genes even demonstrating four types of AS events. For instance, the CCL14 gene displayed significant associations between its AA, AP, ES, and RI events and OS. In order to investigate the functional relationships among these crucial survival-associated events ($p < 0.005$), a gene interaction network was constructed using the STRING Database (Fig. 3B). This network analysis provides valuable insights into potential

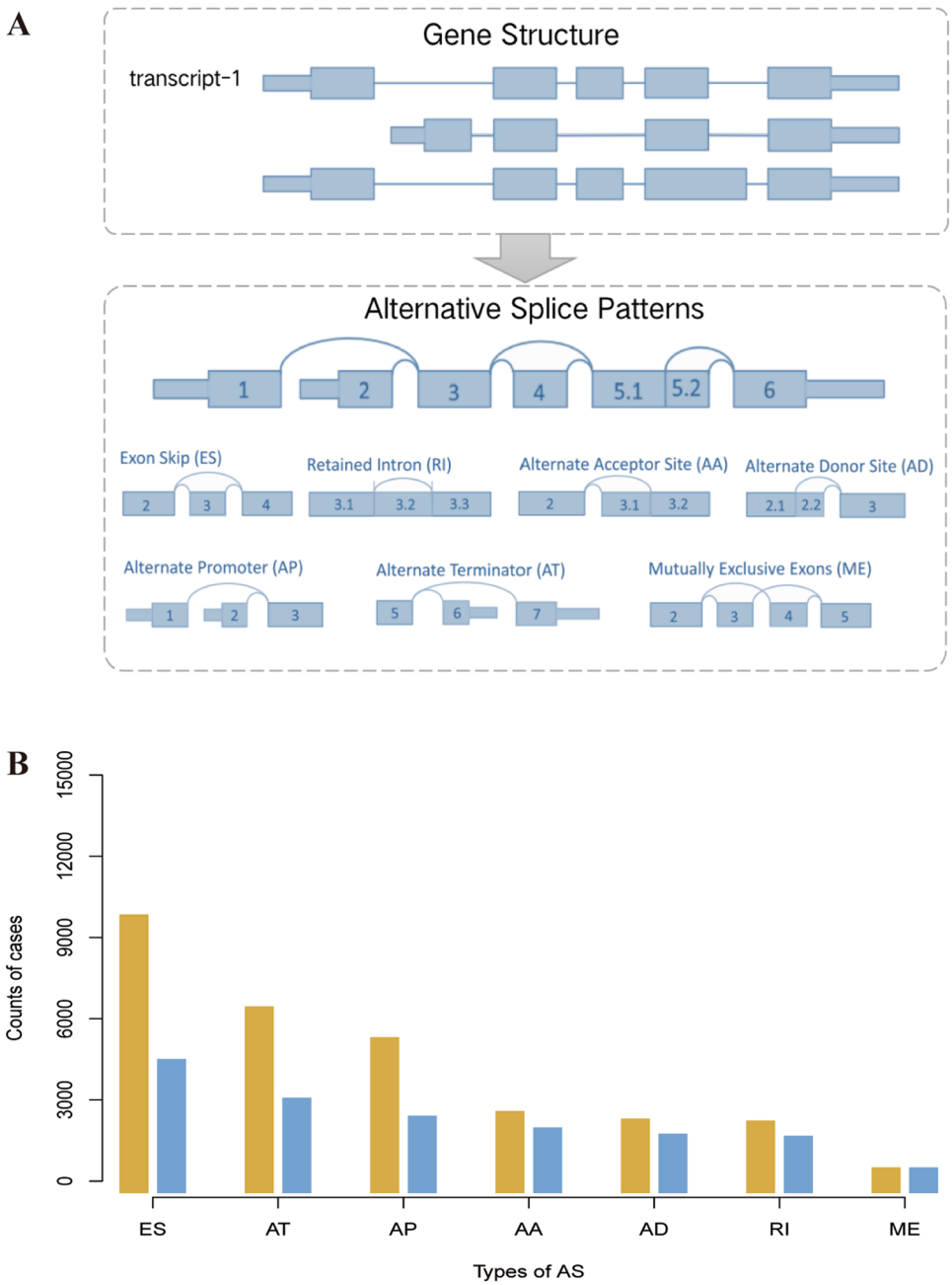

Fig. 1 Schematic representation of AS patterns and AS events in HCC. **A** Diagram illustrating different AS events, including AA, AD, AP, AT, ES, RI, and ME. **B** Count of AS events and associated genes in HCC

molecular interactions and functional connections among the genes involved in these AS events, thereby shedding light on the underlying mechanisms associated with the prognosis of HCC.

These findings provide valuable insights into the prognostic value of AS events in HCC patients and offer clues for further research.

3.2 Cox regression model analysis of prognostic factors in HCC cohort

To uncover autonomous prognostic determinants within individuals diagnosed with HCC, we cautiously handpicked the most momentous AS phenomena associated with survival as potential contenders. We methodically assembled multivariable Cox regression models for each of the seven distinct variants of candidate AS events, aimed at identifying autonomous prognostic indicators. By ingeniously amalgamating the diverse array of candidate AS events from

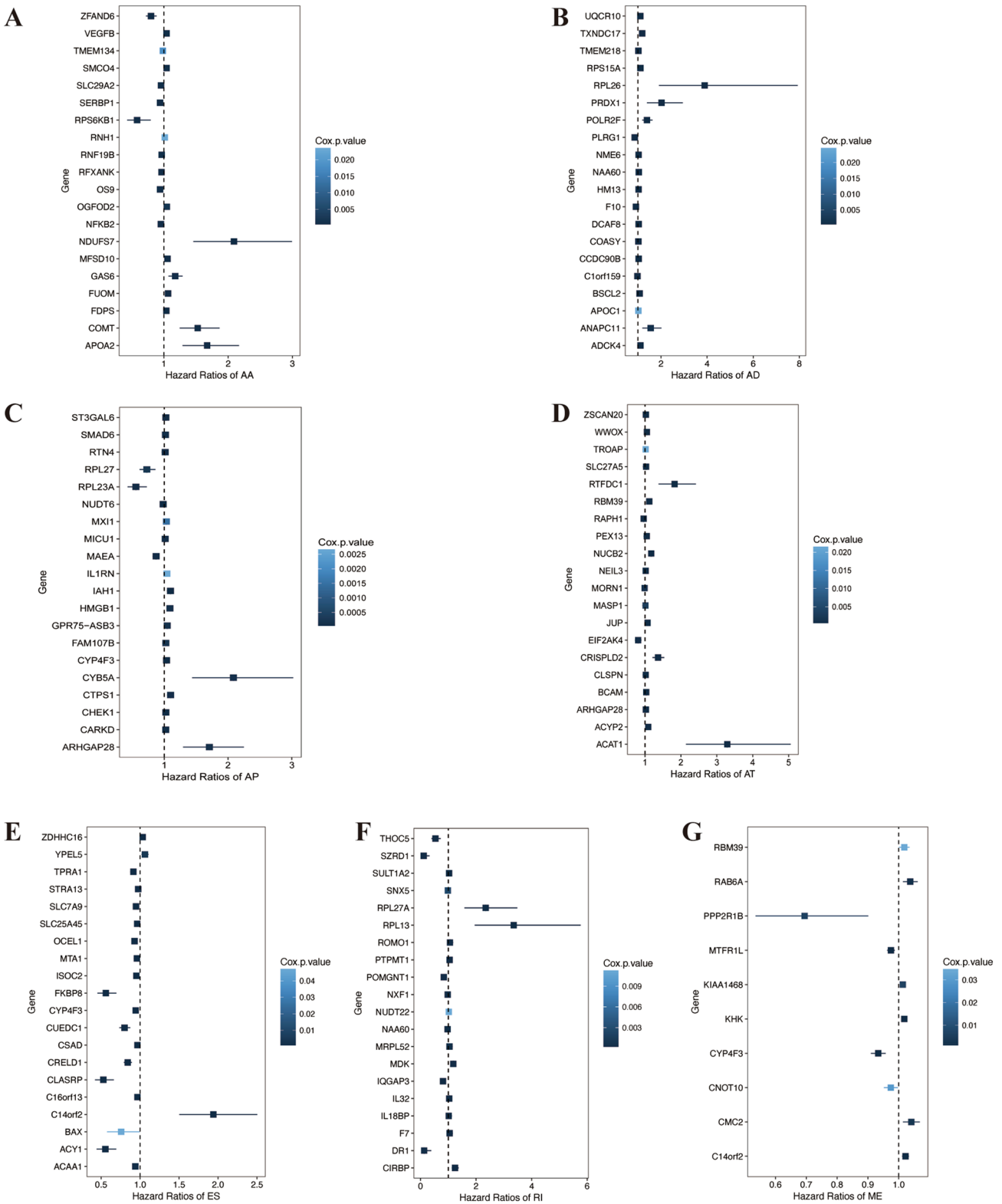

Fig. 2 Forest plots generated to display the subgroup analyses of survival-associated AS events in the HCC cohort. **A**–**G** depicted the hazard ratios (HRs) for the top 20 survival-associated events in different AS types, including AA, AD, AP, AT, ES, RI, and ME events in HCC. The color scale of the circles represented the corresponding p-values, while the horizontal bars represented the 95% confidence intervals (CIs)

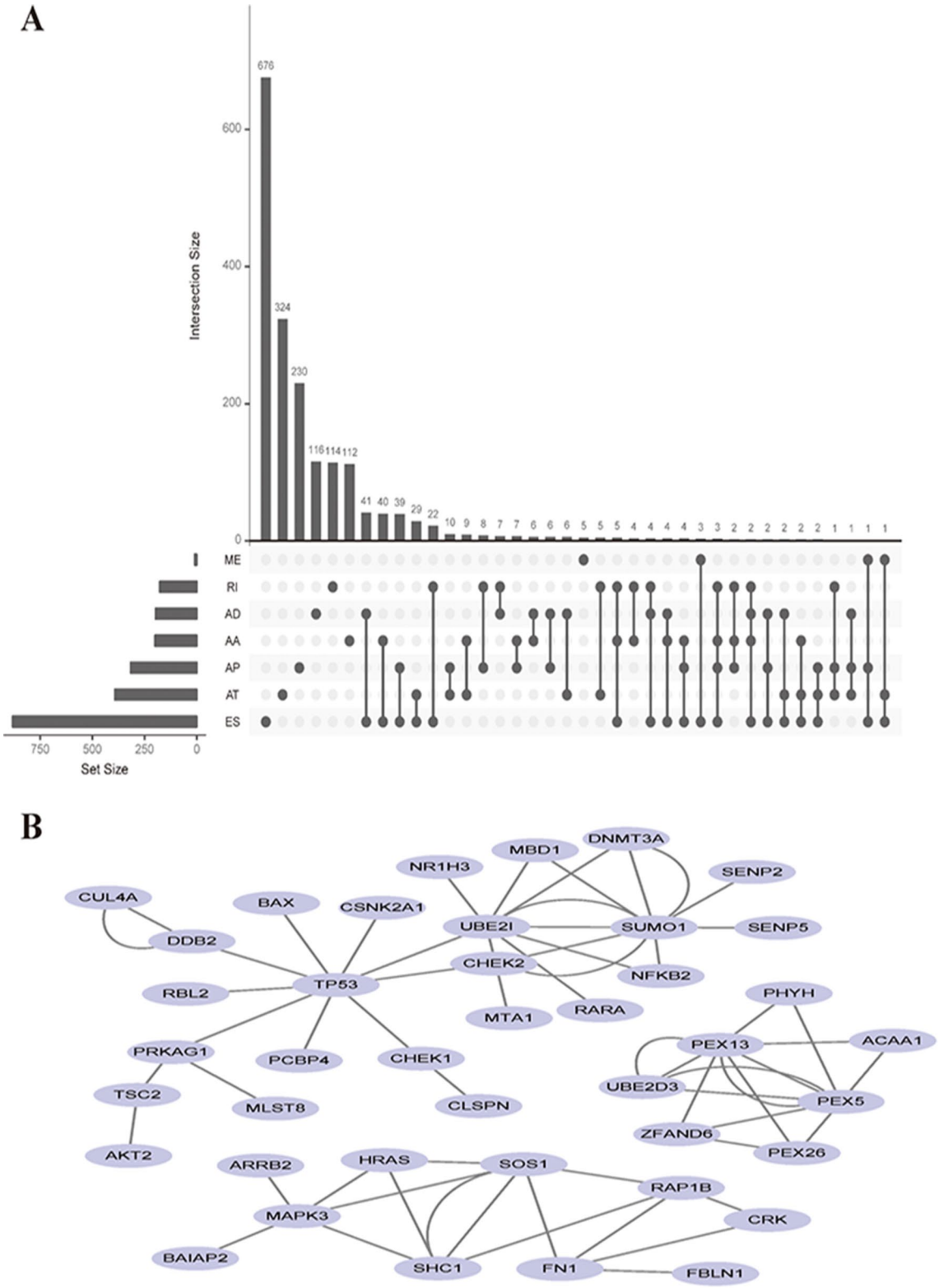

Fig. 3 The analysis of survival-associated AS events in the HCC cohort. **A** UpSet intersection diagram displaying seven types of survival-associated AS events in the HCC cohort. **B** Gene network illustrating the interactions among survival-associated AS events in HCC, created using Cytoscape

these seven categories, we fabricated the ultimate prognostic predictor. Notably, our meticulous examination of the data unequivocally demonstrated the potent prognostic capacities of all seven prognostic models, each predicated on disparate AS event types, in predicting the prognosis of HCC patients (Fig. 4A–G).

Remarkably, it is worth noting that among all the diverse AS events examined (Fig. 4A–G), the prognostic model centered around a solitary AD unveiled the most exceptional performance. Building upon this noteworthy finding, we proceeded to fabricate the ultimate prognostic predictor by amalgamating disparate AS events from all seven distinct types—an endeavor that yielded unprecedented outcomes. It is of paramount significance to emphasize that the performance of this final prognostic predictor surpassed that of each individual splicing pattern, as clearly illustrated in Fig. 4H. Notably, in the analysis of the ROC, the final prognostic predictor exhibited an impressively high AUC of 0.830. Additionally, the AD model and the AA model closely trailed behind, with AUCs of 0.819 and 0.816, respectively, as portrayed in Fig. 4I. These findings serve as compelling evidence that the amalgamation of the various prognostic models within the final combination considerably enhances the predictive accuracy concerning the prognosis of HCC patients. It is also worth mentioning that Table 1 provides a comprehensive inventory of the 15 HCC-specific genes corresponding to the AS events that are encompassed within the final amalgamation of prognostic models.

3.3 Interaction analysis between prognostic-related AS events and splicing factors

In order to determine the splice events associated with survival in HCC patients, we performed survival analysis of splice factors based on gene expression levels. The results showed that 50 splice factors were significantly correlated with OS. Additionally, using Spearman's test, we examined the correlation between the PSI values of the most important AS events and the expression of survival-associated splice factors (Fig. 5A). We found that most adverse survival-associated AS events (red dots) were positively correlated with splice factor expression (gray dots) (red line), while the most favorable prognostic AS events (orange dots) were negatively correlated with splice factor expression (purple line). The high expression of splice factor PRPF38B was associated with poorer patient survival, whereas the high expression of splice factor NONO was associated with better prognosis (Fig. 5B, C). The scatter plot displayed the correlation between splice factor PRPF38B and the AS of RTN4 (Fig. 5D), indicating a positive correlation between high PRPF38B expression and poorer OS. Similarly, the scatter plot showed the correlation between splice factor NONO and the AS of CLSPN (Fig. 5E), suggesting a negative correlation between high NONO expression and favorable prognosis.

3.4 Identification of FTCD as a significant gene for HCC by a comprehensive pan-cancer analysis

Through meticulous analysis of Table s01 and extensive review of relevant literature, we have successfully identified the *FTCD* gene as a compelling candidate that exhibits downregulation in HCC cases and demonstrates a positive correlation with favorable patient prognosis. Subsequently, we delved deeper into our investigation by scrutinizing the expression patterns of *FTCD* across multiple cancer types, including Endometrial Cancer, Cervical Cancer, Miscellaneous Neuroepithelial Tumor, Sarcoma, and Non-Small Cell Lung Cancer. Our findings, as depicted in Fig. 6, illustrate the distinctive and specific expression of *FTCD* in HCC.

Consequently, we leveraged comprehensive data including copy number variation (CNV), RNA-Seq data, methylation status, and clinical information from the HCC cohort in the TCGA database to construct a survival curve for *FTCD*. Our analysis revealed that patients exhibiting high *FTCD* CNVs, elevated *FTCD* expression, and reduced methylation levels experienced more favorable prognoses (as depicted in Fig. 7A). This compelling evidence supports the notion that *FTCD* holds promise as a specific prognostic factor for HCC.

To gain further insights, we meticulously examined the mutation types and positions within the *FTCD* gene. Our investigations indicated that the majority of mutations present were missense mutations, with the most prevalent mutation types being C > T and G > A (as shown in Fig. 7B). Delving into the mutation type distribution of *FTCD* in HCC, we expanded our analysis to include liver cancer data from various databases such as IRKEN, MSK, AMC, and INSERM (Fig. 7C). Strikingly, our findings unveiled the presence of specific structural variations (SV) in the *FTCD* gene solely in HCC cases, while no such SV occurrences were observed in other cancer types (as portrayed in Fig. 6C). This strongly implies a direct association between *FTCD* SV and the development of HCC.

Subsequently, utilizing the Linked Omics of Lots of Indels and Polymorphisms in Cancer (LOLLIPOP) tool, we investigated fusion genes involving *FTCD*. Notably, we identified the specific expression of the E323Sfs*55 fusion in HCC cases,

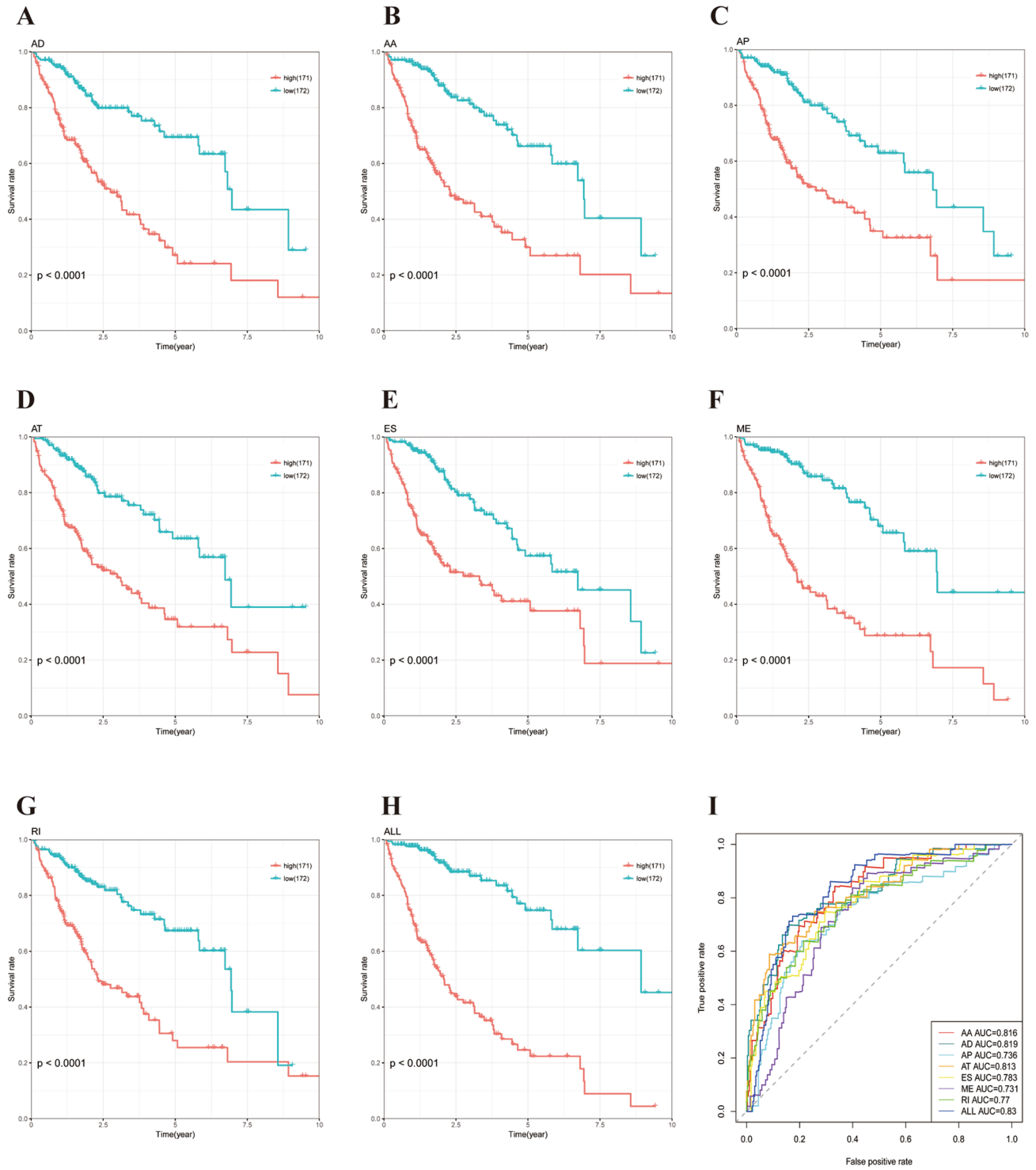

Fig. 4 Kaplan–Meier plot and ROC curves to assess the survival rate for seven types of AS events as prognostic predictors in the HCC cohort. **A**–**G** represents a specific type of AS event, with the high-risk group depicted in red and the low-risk group depicted in blue. **H** A Kaplan–Meier plot to visualize the survival probability over time for the final prognostic predictor in the HCC cohort. The high-risk group is shown in red, while the low-risk group is shown in blue. **I** ROC analysis to evaluate the performance of all prognostic predictors in the HCC cohort. The ROC curves of the prognostic predictors are color-coded to represent different types of AS events

Table 1 HCC-specific genes corresponding to the AS events in the prognostic model

Gene	HR	Lower95	Upper95	*P*	Type	Exons
C14orf2	1.023512	1.007298	1.039987	0.004337	ME	3|4
TMEM218	1.020042	1.003297	1.037067	0.018789	AD	4.3:4.4
FAM107B	0.944023	0.914908	0.974065	0.000313	AP	4
POMGNT1	0.884325	0.793131	0.986004	0.026843	RI	22.2
WWOX	0.968836	0.945908	0.992319	0.009569	AT	13
MFSD10	1.041556	1.004127	1.080379	0.029217	AA	6.1
CLASRP	0.583572	0.429537	0.792847	0.000572	ES	3.2:4:5.1
RPS15A	1.101795	1.024171	1.185302	0.009303	AD	1.2
RAB6A	1.095201	1.051403	1.140823	1.26E-05	ME	5|6
NAA60	0.979703	0.964222	0.995434	0.011631	RI	10.5
NME6	1.024455	1.006149	1.043095	0.008633	AD	1.2:1.3
MTFR1L	0.962417	0.946506	0.978595	6.67E-06	ME	5|6
IL18BP	1.014261	1.003639	1.024995	0.008386	RI	1.7
MAEA	0.897471	0.825776	0.975391	0.01088	AP	1
NUCB2	0.918293	0.844641	0.998369	0.045691	AT	20

whereas the E251* mutation demonstrated higher prevalence across pan cancers (depicted in Figs. 6D and 7D, respectively). These observations suggest that SV events generate fusion genes, thereby altering the functional characteristics of the *FTCD* gene with specific relevance to HCC.

We scrutinized the expression patterns of SV and mRNA z-scores (normalized to diploid samples) for the *FTCD* gene, unveiling elevated expression levels in cases exhibiting increased copy numbers and the presence of SV (as illustrated in Fig. 7E). Additionally, the distribution plot of methylation sites (Fig. 7F) illustrated varying degrees of methylation across different exons. Specifically, low levels of methylation were observed in the initial exons, while the later exons demonstrated higher levels. Notably, distinct differences in methylation were observed among different tumor stages. In stage II and IIIa, aberrantly elevated methylation levels were detected in the initial exons of some patients. Moreover, our investigation into the distribution of *FTCD* gene methylation across different stages of HCC revealed variations in expression levels and methylation extent (as demonstrated in Fig. 7G). Analyzing AS events of the *FTCD* gene, we identified significant differences in expression patterns of the fifth exon among different subtypes. This finding strongly reinforces the association between *FTCD*'s AS patterns and HCC (as depicted in Fig. 7H).We conducted KEGG enrichment analysis and protein–protein interaction network analysis for the *FTCD* gene. The enrichment analysis revealed an enrichment of the *PPAR* pathway, which is associated with tumors. The protein–protein interaction network analysis resulted in three modules that were clustered using K-means algorithm (Fig. 8).

3.5 Validation the role of FTCD in the biological characteristics of liver cancer cells and its molecular mechanisms in vivo and in vitro

In our cell model experiments, a notable decrease in both gene expression and protein levels of *FTCD* was observed in the HCC group compared to the Control group ($p < 0.05$) (as depicted in Fig. 9A–C). Through CCK-8 experiments, we additionally discovered that the HCC group exhibited the highest cell proliferation capacity, while the Control group displayed the weakest (Fig. 9D). Remarkably, the *FTCD*-overexpressing group (FTCD group) demonstrated a significantly attenuated cell proliferation ability in comparison to the HCC group, albeit still higher than that of the Control group ($p < 0.05$). This finding strongly suggests the inhibitory role of the *FTCD* gene in regulating cell proliferation. Furthermore, our investigation delved into the expression levels of genes associated with the PPAR/PI3K/AKT/mTOR pathway, as shown in Fig. 8. Notably, by overexpressing *FTCD* (FTCD group) in BEL-7402 cells, we documented a significant downregulation in the expression of PPARδ, PIK3CA, and AKT, along with an elevation in the expression of the upstream negative regulator PTEN ($p < 0.05$) (Fig. 9A–C). These compelling findings reinforce the hypothesis that *FTCD* may exert its inhibitory effect on the biological characteristics of liver cancer cells through the precise regulation of the *PPAR/PI3K/AKT/mTOR* pathway.

In the mice model, researchers introduced liver cancer cells transfected with *FTCD* overexpression plasmids into mice to establish a tumor-bearing mice model. The growth rate and size of the tumors were carefully observed and compared among different groups, while liver tissues were collected for pathological examination. Immunohistochemistry was

Fig. 5 A correlation network to visualize the relationship between splicing factors and genes in the HCC cohort. **A** The correlation network ▶ between the expression levels of survival-associated splicing factors and the Percent Spliced In (PSI) values of AS genes in the HCC cohort. **B**, **C** Kaplan–Meier curves generated to assess the survival probability over time for the splicing factors *PRPF38B* and *NONO*, respectively. The high-expression group is represented by the red curve, while the low-expression group is represented by the blue curve in the HCC cohort. **D** The correlation between the expression level of the splicing factor *PRPF38B* and the PSI value of the alternative splicing gene *RTN4*. **E** The correlation between the expression level of the splicing factor *NONO* and the PSI value of the alternative splicing gene *CLSPN*

employed to evaluate the staining of the FTCD protein in the mice liver tissues. Significantly, the content of FTCD protein in the liver tissues of the tumor-bearing mice model (H group) was found to be lower than that in the CK group ($p < 0.01$). However, in the *FTCD* overexpression tumor-bearing mice model (F group), the FTCD protein content in the liver tissues was higher than that in the H group ($p < 0.05$) (as demonstrated in Fig. 9E). Furthermore, using RT-PCR detection, we observed that the expression level of *FTCD* in the control group (CK group) surpassed that in both the tumor-bearing mice model (H group) and the *FTCD* overexpression tumor-bearing mice model (F group) ($p < 0.05$) (Fig. 9F). Consistently, western blot analysis revealed that the content of FTCD protein in the control group (CK group) was higher compared to both the H group and F group ($p < 0.05$) (Fig. 9G, H), corroborating the results obtained from the pathological examination. Importantly, these findings highlight the crucial role of *FTCD* in liver cancer and its correlation with molecular mechanisms.

In summary, our study encompassed several key steps to provide a comprehensive understanding of the significance of *FTCD* in liver cancer and its associated molecular mechanisms. Initially, we performed a genome-wide analysis using RNA-seq data from TCGA to investigate prognostic-associated AS events within a cohort of 343 liver cancer patients. Through comprehensive Cox proportional hazards regression analysis, we established a prognostic prediction model. By examining the correlation between survival-associated AS events and splicing factors, we constructed a splicing network to elucidate the underlying regulatory mechanisms. Subsequently, we identified a notable association between *FTCD* and prognosis, prompting further exploration of AS patterns within the FTCD gene. To validate the inhibitory effect of *FTCD* on the biological characteristics of liver cancer cells, we employed both mice models and cell models. The findings from these experiments supported the notion that *FTCD* exerts its inhibitory influence by modulating the *PPAR/PI3K/AKT/mTOR* pathway.

In essence, this comprehensive investigation sheds light on the pivotal role of *FTCD* in liver cancer and provides insights into the intricate molecular mechanisms underlying its function.

4 Discussion

HCC is the primary type of liver cancer, often associated with chronic infections caused by the hepatitis B virus (HBV) and hepatitis C virus (HCV). Additionally, it can arise from long-term liver disease, like inflammation, alcoholic and non-alcoholic liver cirrhosis. These factors significantly elevate the risk of developing liver cancer. More than three decades ago, researchers made a significant breakthrough by identifying alterations in RNA splicing in cancer. In the case of liver cancer, numerous genes involved in RNA splicing, such as *DNMT3b*, *AURKB*, *MDM2*, undergo notable modifications [23]. In vitro studies have revealed that these genes play a pivotal role in promoting cellular proliferation, inhibiting apoptosis, and facilitating cellular transformation. Furthermore, RNA splicing plays a crucial role in the expression of HBV and HCV, due to the fact that numerous viruses exploit the cellular splicing machinery to manipulate the splicing of their viral RNA [24]. Aberrant splicing leads to the production of mRNA isoforms implicated in the development and malignancy of liver cancer [25]. Several studies have aimed to establish a connection between AS signatures and the prognosis of HCC [26–28]. In a recent study, a comprehensive reanalysis of RNA splicing alterations in the liver revealed the identification of approximately 45,000 AS events. This finding highlights the extensive complexity and diversity of splicing patterns occurring in liver cells [26]. The researchers of this study also assessed the expression levels of splicing factors in the analyzed samples and observed alterations in the expression of 26 specific splicing factors. These findings provide compelling evidence that substantial changes in RNA splicing take place during the progression of liver cancer. Such insights contribute to our understanding of the underlying pathological mechanisms involved in liver cancer development.

Through the analysis of data from TCGA, we conducted a study aimed at investigating AS events and regulatory splicing factors in HCC. Our objective was to gain a deeper understanding of the differential RNA splicing patterns in this context. As a result, we identified a total of 3164 splicing events that exhibit associations with the survival of HCC patients. Notably, the top 20 survival-associated splicing events frequently demonstrate a correlation with poor

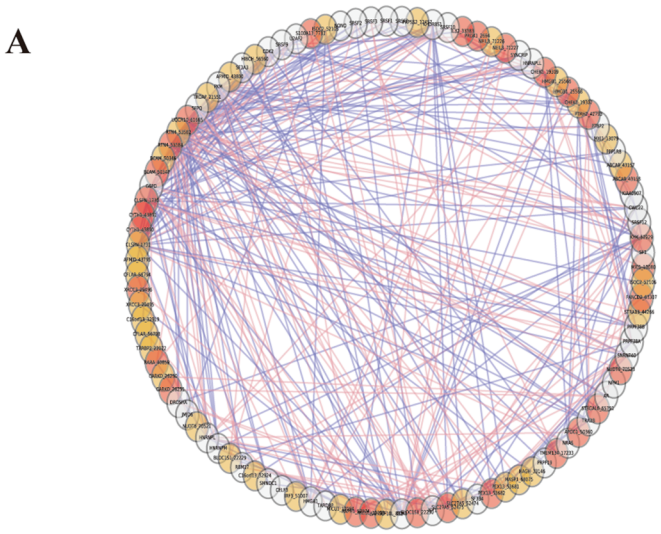
A

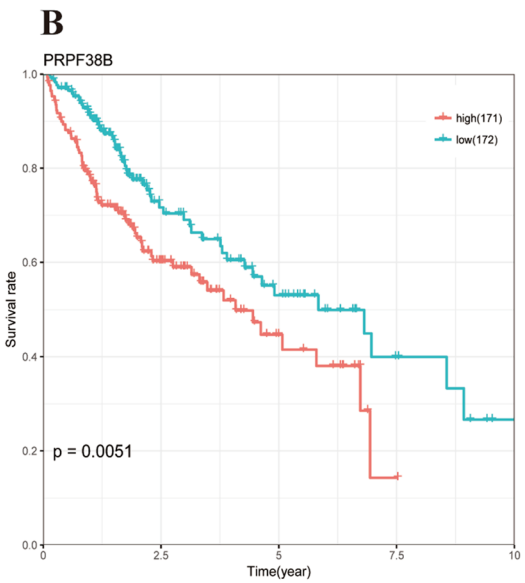
B
PRPF38B
high(171)
low(172)
Survival rate
p = 0.0051
Time(year)

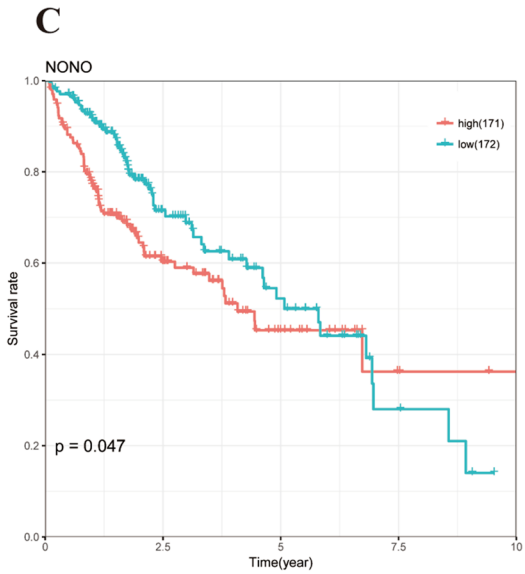
C
NONO
high(171)
low(172)
Survival rate
p = 0.047
Time(year)

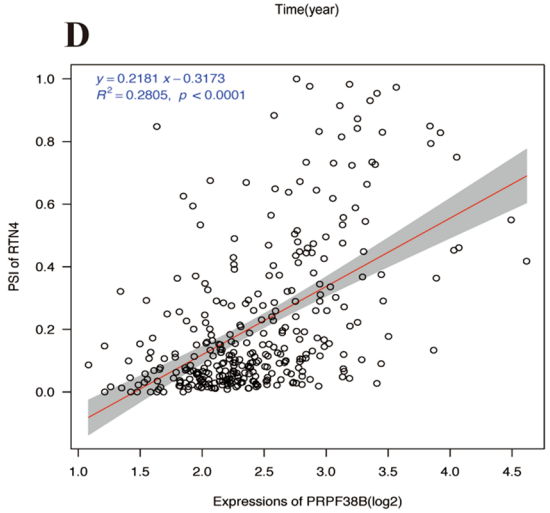
D
y = 0.2181 x − 0.3173
R² = 0.2805, p < 0.0001
PSI of RTN4
Expressions of PRPF38B(log2)

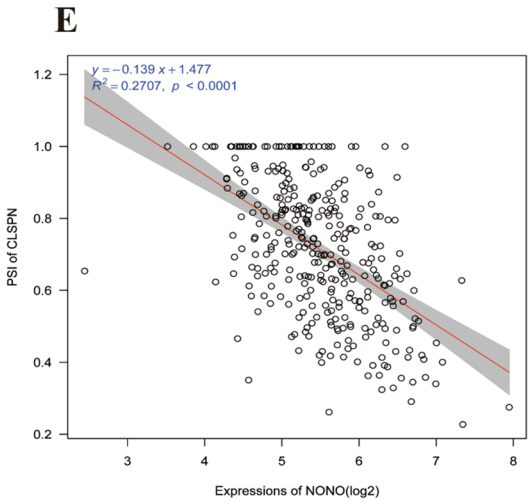
E
y = −0.139 x + 1.477
R² = 0.2707, p < 0.0001
PSI of CLSPN
Expressions of NONO(log2)

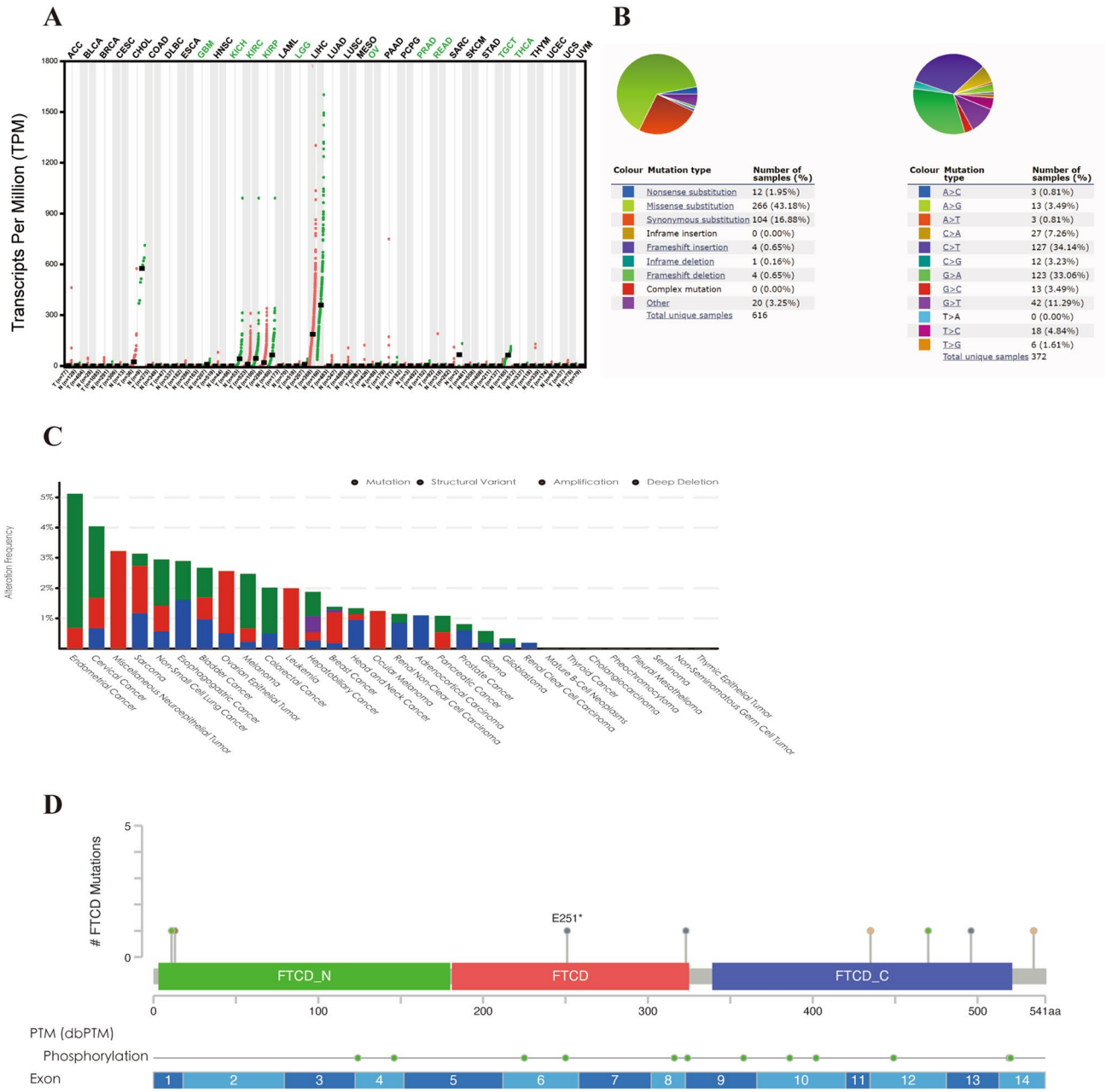

Fig. 6 The pan-cancer analysis of *FTCD* demonstrates its specific expression in the liver. **A** Displays the TPM (Transcripts Per Million) statistics for the gene. **B**, **C** provide statistics on the types of mutations. **D** Illustrates the mutation sites of *FTCD* in pan-cancer

prognosis. Furthermore, we developed a prognostic model based on the differential splicing patterns of 15 genes, which effectively enables the stratification of risk levels in HCC patients. Another significant discovery from our study is the presence of a splicing-associated network that interconnects the expression of splicing factors and specific splicing events in HCC patients. Previous studies have indicated that certain splicing variants and cancer-specific splicing events can serve as valuable diagnostic, predictive, and prognostic biomarkers for HCC. Additionally, recent research has provided evidence that abnormal splicing events contribute to the development and progression of HCC by regulating the expression of genes involved in energy metabolism and DNA damage response [20, 29–31]. However, it is important to note that the current understanding in this field primarily relies on studies employing small sample sizes and exon microarray analysis. In contrast, high-throughput sequencing analysis has emerged as a recognized key technology for investigating genetic abnormalities in splice isoforms and splice sites. Therefore,

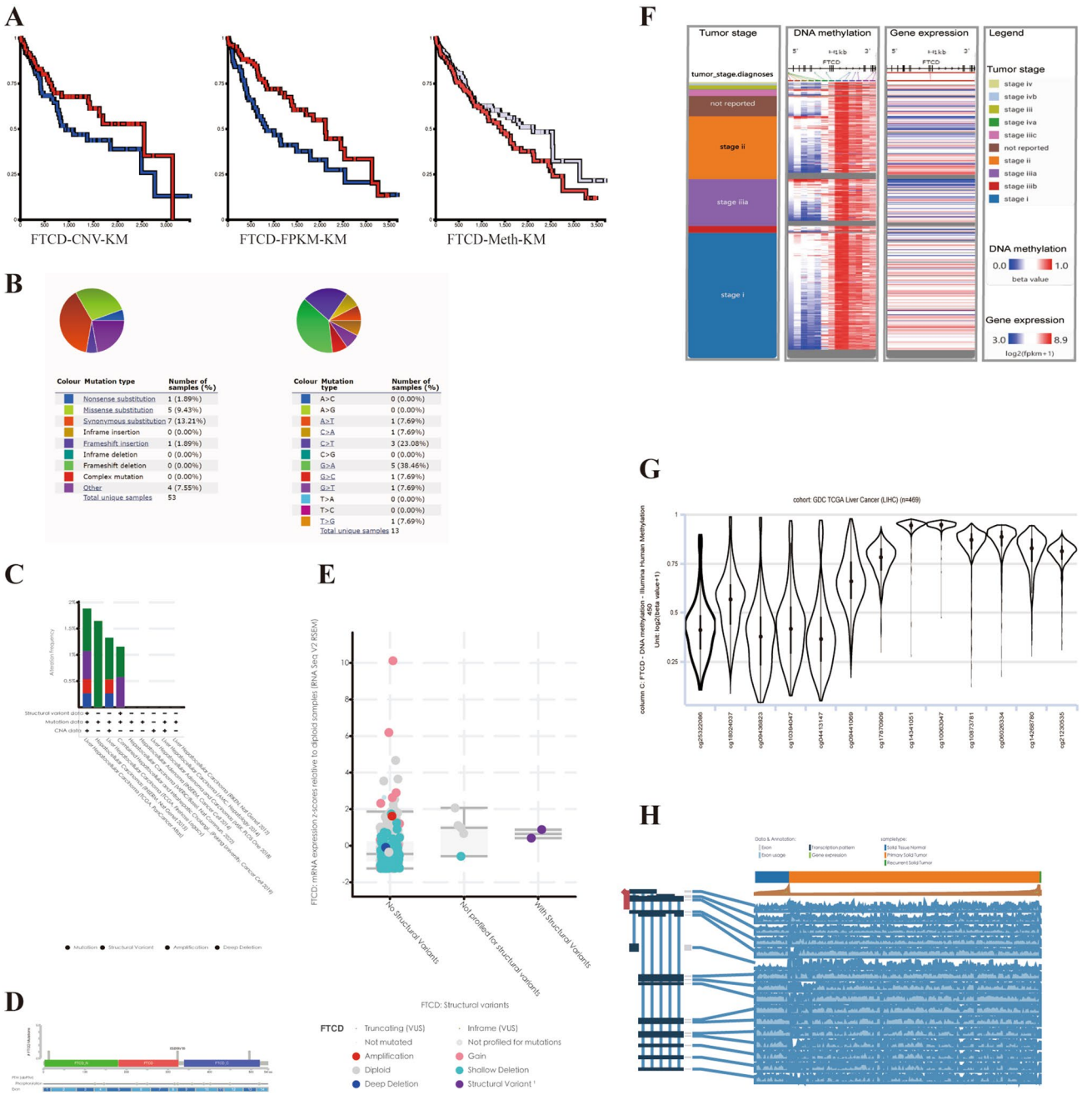

Fig. 7 HCC multi-omics prognostic features. **A** Kaplan–Meier plot illustrating the survival probability over time based on the prognostic predictors of CNV, FPKM and methylation of *FTCD*. The high-expression group is represented by the red curve, while the low-expression group is represented by the blue curve. **B**, **C** Present statistics on the types of mutations. **D** Displays the mutation sites. **E** Shows the distribution of mutation types in terms of expression levels. **F** Represents the distribution of expression levels for methylation sites. **G** Illustrates the distribution of expression levels for methylated sites. **H** Depicts the distribution of AS expression levels

attaining a comprehensive understanding of abnormal splicing patterns is essential for the exploration of novel therapeutic strategies for HCC.

FTCD is an enzyme that relies on folate for its activity. It plays a crucial role in catalyzing a reaction within the histidine degradation pathway. Notably, *FTCD* exhibits high expression levels in the liver. Previous research has demonstrated that this enzyme is involved in the regulation of liver enlargement and dysfunction induced by starvation. Specifically, *FTCD* achieves this regulatory function by inhibiting the *mTORC1* pathway [32]. However, there is limited research on the association between *FTCD* and the prognosis of HCC. Our study has shown that *FTCD* was significantly downregulated

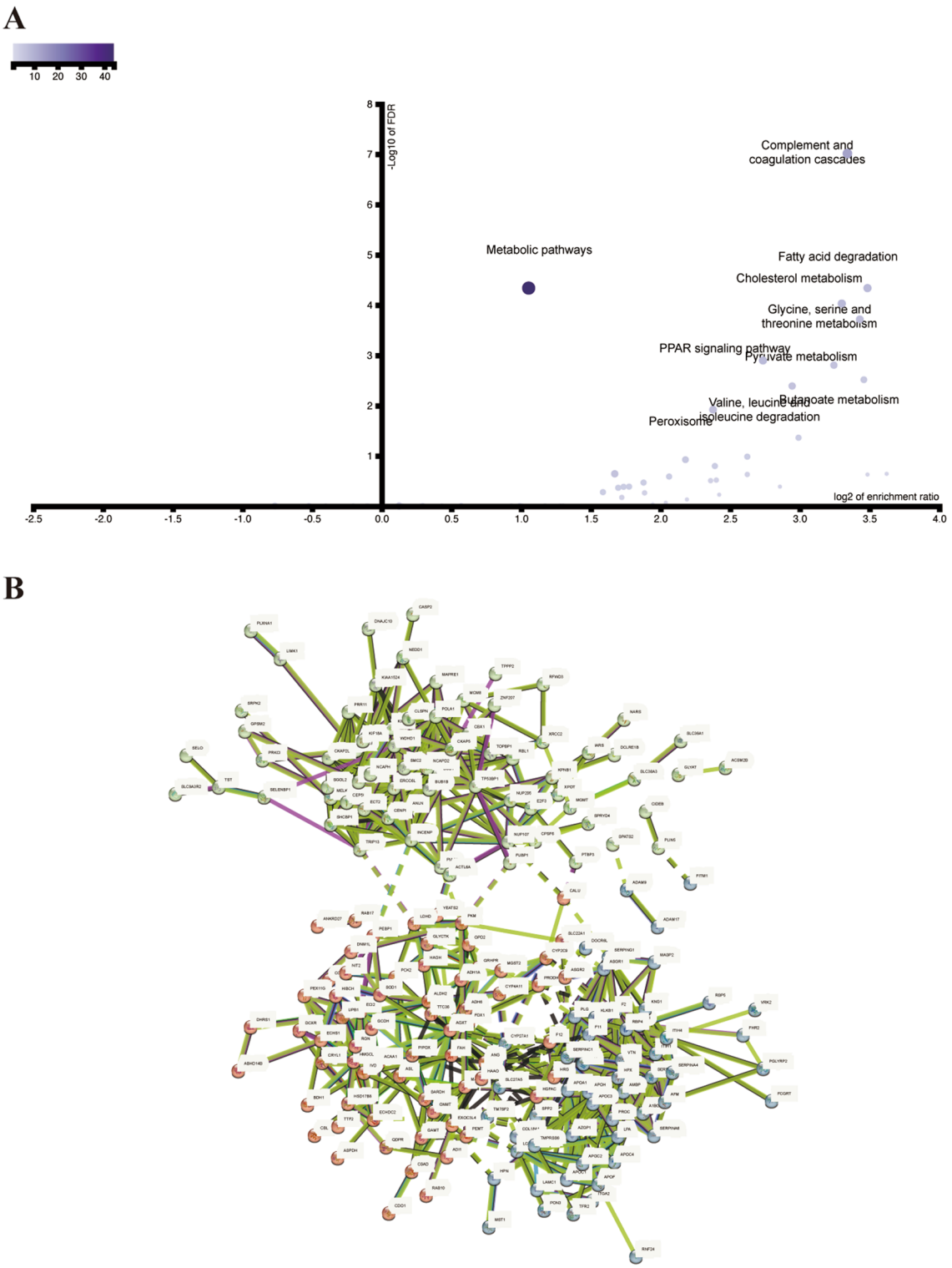

Fig. 8 KEGG enrichment analysis and protein–protein interaction (PPI) network analysis of co-expressed genes with *FTCD*. **A** Enrichment analysis reveals the enrichment of the *PPAR* pathway, which is associated with tumors. **B** PPI analysis using K-means clustering results in the formation of three modules

in HCC tissues compared to adjacent non-cancerous tissues, and lower *FTCD* levels were associated with poorer prognosis in HCC patients, which is consistent with the previous findings [33]. The *PPAR/PI3K/AKT/mTOR* signaling pathway was found to be influenced by *FTCD* in HCC by a murine liver-specific *FTCD* knockout model [34]. This study found that

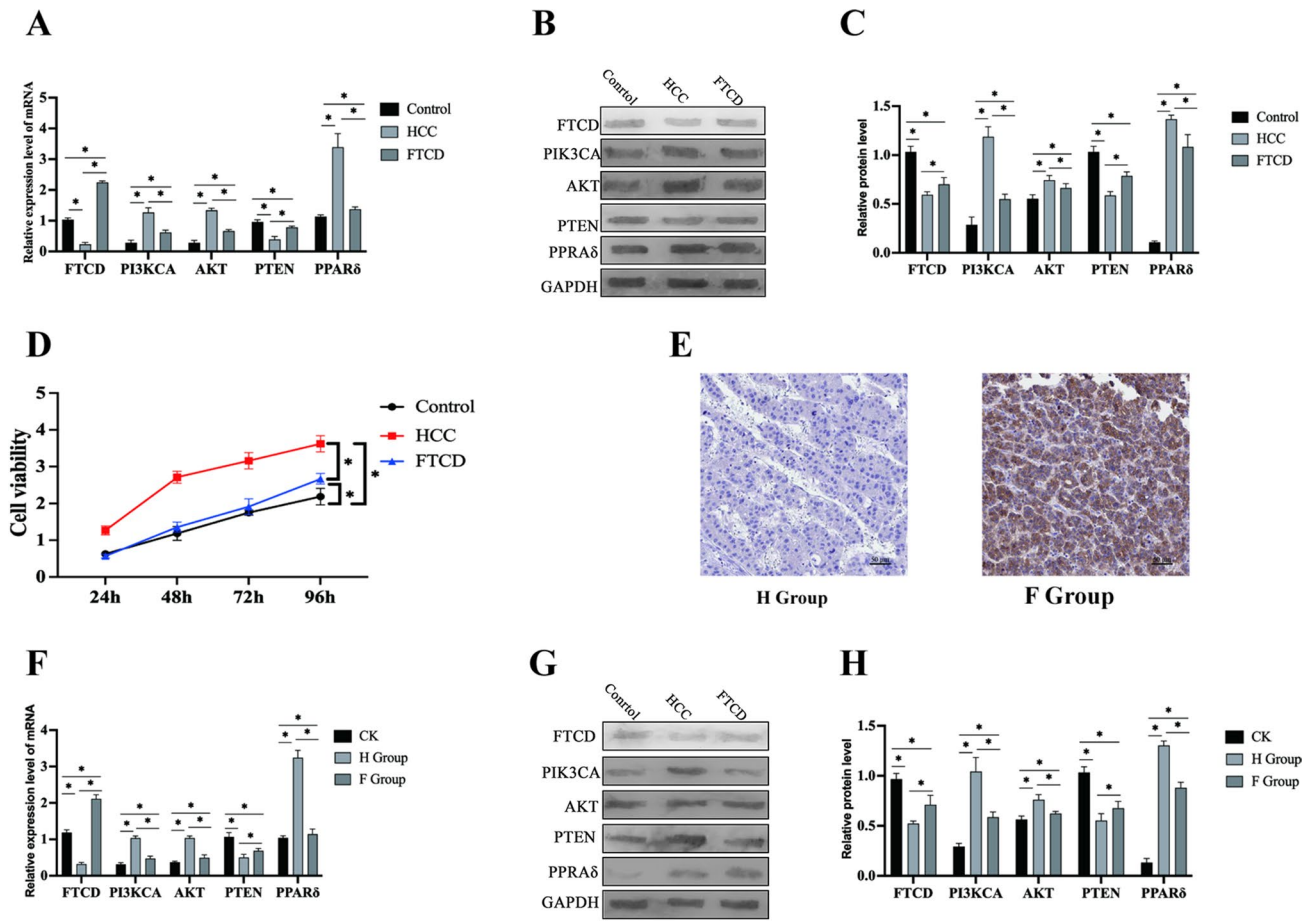

Fig. 9 Validation the role of *FTCD* in cell model and mice model. **A** qPCR results of *FTCD*, *PPARδ*, *PIK3CA*, *AKT*, and *PTEN* genes in the cell model. **B**, **C** Western blot results of FTCD, PPARδ, PIK3CA, AKT, and PTEN in the cell model. **D** Cell proliferation results using the CCK-8 assay. **E** Immunohistochemistry results in the mice model. **F** qPCR results of *FTCD*, *PPARδ*, *PIK3CA*, *AKT*, and *PTEN* genes in the mice model. **G**, **H** Western blot results of FTCD, PPARδ, PIK3CA, AKT, and PTEN in the mice model

loss of *FTCD* upregulates *PPARγ* and *SREBP2* through modulation of the *PTEN/AKT/mTOR* signaling pathway, leading to lipid accumulation and hepatocarcinogenesis. Another study also indicated that overexpression of *FTCD* can lead to an increase in PTEN protein levels in HCC cells, while decreasing the levels of *PI3K*, total *AKT* and phosphorylated *AKT* proteins, suggesting involvement of the *PI3K/AKT* pathway [35]. Thus, we conducted an investigation into the role of *FTCD* in HCC and discovered that its overexpression leads to the downregulation of *PPARδ*, *PIK3CA*, and *AKT*, while concurrently upregulating the expression of the upstream negative regulator PTEN in HCC. Collectively, these findings highlight the regulatory role of *FTCD* in the *PPAR/PI3K/AKT/mTOR* signaling pathway in HCC. Moreover, this study identifies *FTCD* as a potential prognostic factor for HCC, based on the comprehensive analysis of these results.

Our study employed splice network analysis to uncover the interplay between splice factors and AS events in HCC. Our findings demonstrated a positive correlation between the majority of adverse prognostic AS events and the expression of splice factors in HCC, while favorable prognostic AS events exhibited a negative correlation with splice factor expression. The splicing process is intricately regulated by splice factors that selectively bind to specific splicing regulatory elements within genes. In our investigation, we specifically identified the *FTCD* gene as being associated with HCC prognosis and conducted a comprehensive analysis of *FTCD* AS events. Additionally, we conducted experiments using both mouse and cell models to validate the inhibitory effect of *FTCD* on the biological characteristics of liver cancer cells through the regulation of the *PPAR/PI3K/AKT/mTOR* pathway. This study enhances our understanding of the relationship between splice events and splice factors in HCC, and contributes to the elucidation of potential mechanisms by which *FTCD* influences tumor prognosis through AS.

Author contributions Yanli Zhang led the study's conception, design, and manuscript drafting, and is the corresponding author. Wenxing Li conducted data analysis and contributed to the manuscript's writing. Mengyi Sun was involved in data collection and experimental validation of the FTCD gene. Lisheng Zhang provided guidance on the study's design and critically revised the manuscript. All authors read and approved the final manuscript.

Data availability The original data could be obtained from the corresponding author.

Declarations

Ethics approval and consent to participate The study was approved by the ethics committee of Huazhong Agricultural University (No. [2023]020423).

Competing interests The authors declare no competing interests.

5. References

1. Freddie B, Jacques F, Soerjomataram I, Siegel RL. Global cancer statistics 2018: GLOBOCAN estimates of incidence and mortality worldwide for 36 cancers in 185 countries. CA Cancer J Clin. 2018;68:394.
2. Gilles H, Garbutt T, Landrum J. Hepatocellular carcinoma. Crit Care Nurs Clin North Am. 2022;34(3):289–301.
3. Zhang Q, He Y, Luo N, Patel SJ, Han Y, Gao R, Modak M, Carotta S, Haslinger C, Kind D, Peet GW, Zhong G, Lu S, Zhu W, Mao Y, Xiao M, Bergmann M, Hu X, Kerkar SP, Vogt AB, Pflanz S, Liu K, Peng J, Ren X, Zhang Z. Landscape and dynamics of single immune cells in hepatocellular carcinoma. Cell. 2019;179(4):829-845.e20.
4. Anwanwan D, Singh SK, Singh S, Saikam V, Singh R. Challenges in liver cancer and possible treatment approaches. Biochimica et Biophysica Acta (BBA) Reviews on Cancer. 2019;1873:188314.
5. Le KQ, Prabhakar BS, Hong WJ, Li LC. Alternative splicing as a biomarker and potential target for drug discovery. Acta Pharmacol Sin. 2015;36(10):1212–8.
6. Floor SN, Doudna JA. Tunable protein synthesis by transcript isoforms in human cells. eLife. 2016;5.
7. Lee Y, Rio DC. Mechanisms and regulation of alternative pre-mRNA splicing. Annu Rev Biochem. 2015;84:291–323.
8. Liu Y, Gonzàlez-Porta M, Santos S, Brazma A, Marioni JC, Aebersold R, Venkitaraman AR, Wickramasinghe VO. Impact of alternative splicing on the human proteome. Cell Rep. 2017;20(5):1229–41.
9. Baralle FE, Giudice J. Alternative splicing as a regulator of development and tissue identity. Nat Rev Mol Cell Biol. 2017;18(7):437–51.
10. Kalsotra A, Cooper TA. Functional consequences of developmentally regulated alternative splicing. Nat Rev Genet. 2011;12(10):715–29.
11. Nilsen TW, Graveley BR. Expansion of the eukaryotic proteome by alternative splicing. Nature. 2010;463(7280):457–63.
12. Lee SE, Alcedo KP, Kim HJ, Snider NT. Alternative splicing in hepatocellular carcinoma. Cell Mol Gastroenterol Hepatol. 2020;10(4):699–712.
13. Xu K, Wu T, Xia P, Chen X, Yuan Y. Alternative splicing: a bridge connecting NAFLD and HCC. Trends Mol Med. 2023;29(10):859–72.
14. Marin JJG, Reviejo M, Soto M, Lozano E, Asensio M, Ortiz-Rivero S, Berasain C, Avila MA, Herraez E. Impact of alternative splicing variants on liver cancer biology. Cancers (Basel). 2021;14(1):18.
15. Zhang YF, Wang YX, Zhang N, Lin ZH, Wang LR, Feng Y, Pan Q, Wang L. Prognostic alternative splicing regulatory network of RBM25 in hepatocellular carcinoma. Bioengineered. 2021;12(1):1202–11.
16. Zhou HZ, Li F, Cheng ST, Xu Y, Deng HJ, Gu DY, Wang J, Chen WX, Zhou YJ, Yang ML, Ren JH, Zheng L, Huang AL, Chen J. DDX17-regulated alternative splicing that produced an oncogenic isoform of PXN-AS1 to promote HCC metastasis. Hepatology (Baltimore, MD). 2022;75(4):847–65.
17. Su T, Zhang N, Wang T, Zeng J, Li W, Han L, Yang M. Super enhancer-regulated LncRNA LINC01089 induces alternative splicing of DIAPH3 to drive hepatocellular carcinoma metastasis. Can Res. 2023;83(24):4080–94.
18. Obeng EA, Stewart C, Abdel-Wahab O. Altered RNA processing in cancer pathogenesis and therapy. Cancer Discov. 2019;9(11):1493–510.
19. Jin YJ, Byun S, Han S, Chamberlin J, Kim D, Kim MJ, Lee Y. Differential alternative splicing regulation among hepatocellular carcinoma with different risk factors. BMC Med Genomics. 2019;12(Suppl 8):175.
20. Yu L, Kim J, Jiang L, Feng B, Ying Y, Ji KY, Tang Q, Chen W, Mai T, Dou W, Zhou J, Xiang LY, He YF, Yang D, Li Q, Fu X, Xu Y. MTR4 drives liver tumorigenesis by promoting cancer metabolic switch through alternative splicing. Nat Commun. 2020;11(1):708.
21. Luo C, Cheng Y, Liu Y, Chen L, Liu L, Wei N, Xie Z, Wu W, Feng Y. SRSF2 regulates alternative splicing to drive hepatocellular carcinoma development. Can Res. 2017;77(5):1168–78.
22. Solans A, Estivill X, de la Luna S. Cloning and characterization of human FTCD on 21q22.3, a candidate gene for glutamate formiminotransferase deficiency. Cytogenet Cell Genet. 2000;88(1–2):43–9.

23. Berasain C, Goñi S, Castillo J, Latasa MU, Prieto J, Avila MA. Impairment of pre-mRNA splicing in liver disease: mechanisms and consequences. World J Gastroenterol. 2010;16(25):3091–102.
24. Karakama Y, Sakamoto N, Itsui Y, Nakagawa M, Tasaka-Fujita M, Nishimura-Sakurai Y, Kakinuma S, Oooka M, Azuma S, Tsuchiya K, Onogi H, Hagiwara M, Watanabe M. Inhibition of hepatitis C virus replication by a specific inhibitor of serine-arginine-rich protein kinase. Antimicrob Agents Chemother. 2010;54(8):3179–86.
25. Yosudjai J, Wongkham S, Jirawatnotai S, Kaewkong W. Aberrant mRNA splicing generates oncogenic RNA isoforms and contributes to the development and progression of cholangiocarcinoma. Biomed Rep. 2019;10(3):147–55.
26. Tremblay MP, Armero VE, Allaire A, Boudreault S, Martenon-Brodeur C, Durand M, Lapointe E, Thibault P, Tremblay-Létourneau M, Perreault JP, Scott MS, Bisaillon M. Global profiling of alternative RNA splicing events provides insights into molecular differences between various types of hepatocellular carcinoma. BMC Genomics. 2016;17(1):683.
27. Li S, Hu Z, Zhao Y, Huang S, He X. Transcriptome-wide analysis reveals the landscape of aberrant alternative splicing events in liver cancer. Hepatology (Baltimore, MD). 2019;69(1):359–75.
28. Xiong Y, Yang G, Wang K, Riaz M, Xu J, Lv Z, Zhou H, Li Q, Li W, Sun J, Tao T, Li J. Genome-wide transcriptional analysis reveals alternative splicing event profiles in hepatocellular carcinoma and their prognostic significance. Front Genet. 2020;11:879.
29. Ma WK, Voss DM, Scharner J, Costa ASH, Lin KT, Jeon HY, Wilkinson JE, Jackson M, Rigo F, Bennett CF, Krainer AR. ASO-based PKM splice-switching therapy inhibits hepatocellular carcinoma growth. Can Res. 2022;82(5):900–15.
30. Dayton TL, Gocheva V, Miller KM, Israelsen WJ, Bhutkar A, Clish CB, Davidson SM, Luengo A, Bronson RT, Jacks T, Vander Heiden MG. Germline loss of PKM2 promotes metabolic distress and hepatocellular carcinoma. Genes Dev. 2016;30(9):1020–33.
31. Hu G, Wang S, Wang Y, Gao Y, Zhu H, Liu M, Xu N, Wang L. Clinical and functional significance of CHK1-S, an alternatively spliced isoform of the CHK1 gene, in hepatocellular carcinoma. J Cancer. 2020;11(7):1792–9.
32. Zhang W, Wu C, Ni R, Yang Q, Luo L, He J. Formimidoyltransferase cyclodeaminase prevents the starvation-induced liver hepatomegaly and dysfunction through downregulating mTORC1. PLoS Genet. 2021;17(12): e1009980.
33. Identification of novel immunohistochemical tumor markers for primary hepatocellular carcinoma; clathrin heavy chain and formiminotransferase cyclodeaminase, Hepatology (Baltimore, Md.) 48 (2010).
34. Wang S, Zhou Y, Yu R, Ling J, Li B, Yang C, Cheng Z, Qian R, Lin Z, Yu C, Zheng J, Zheng X, Jia Q, Wu W, Wu Q, Chen M, Yuan S, Dong W, Shi Y, Jansen R, Yang C, Hao Y, Yao M, Qin W, Jin H. Loss of hepatic FTCD promotes lipid accumulation and hepatocarcinogenesis by upregulating PPARγ and SREBP2. JHEP Rep. 2023;5(10): 100843.
35. Chen J, Chen Z, Huang Z, Yu H, Li Y, Huang W. Formiminotransferase cyclodeaminase suppresses hepatocellular carcinoma by modulating cell apoptosis, DNA damage, and phosphatidylinositol 3-kinases (PI3K)/Akt signaling pathway. Med Sci Monitor. 2019;25:4474–84.